A Multi-Analytical Study of Egyptian Funerary Artifacts from Three Portuguese Museum Collections

Nick Schiavon [1,*], **Patricia Panganiban** [1], **Sara Valadas** [1], **Carlo Bottaini** [1], **Cristina Barrocas Dias** [1,2], **Ana Manhita** [1] **and Antonio Candeias** [1,2]

[1] Hercules Laboratory, University of Evora, 7000-809 Évora, Portugal; pcmhpanganiban@gmail.com (P.P.); svaladas@uevora.pt (S.V.); carlo@uevora.pt (C.B.); cmbd@uevora.pt (C.B.D.); anaccm@uevora.pt (A.M.); candeias@uevora.pt (A.C.)

[2] Department of Chemistry, School of Sciences and Technology, University of Évora, 7000-671 Évora, Portugal

[*] Correspondence: schiavon@uevora.pt; Tel.: +351-939007452

Abstract: A diachronic, multi-analytical approach combining EDXRF, μFTIR, μRaman, SEM-EDS, and Py-GC/MS has been adopted with the aim to study for the first time the painting materials used to decorate Egyptian funerary masks and sarcophagi ranging from the Late Period to the Roman Period and stored in the Archaeological National Museum (MNA) and the Carmo Archaeological Museum (MAC) of Lisbon and the Natural History Museum of the University in Oporto (MNH-FCUP). Results indicate that yellow and red ochres, realgar, cinnabar, Egyptian blue, and Egyptian green were used as pigments while chalk served as the preparatory layer. Over the 1000-year time-line of the studied artifacts, the palette remained remarkably consistent with previous findings as exemplified by cinnabar being used for red pigments in samples only dated after the Ptolemaic period. The presence of Sn in Egyptian blue and Egyptian green pigments used in one sample sug-gests the use of recycled bronze scraps during pigment production. Black pigments in two Late Period masks were found to be produced by mixing Egyptian blue with red ochre suggesting either a hitherto unknown method for production of purple pigments in the Egyptian palette or, alterna-tively, an attempt to create a specific hue or shade of dark brown or black. The results of this study contribute to further expand the database of Ancient Egyptian painting materials while at the same time helping to valorize three important Egyptian collections in Portugal.

Keywords: Egyptian pigments; binders; XRF; μFTIR; μRaman; SEM-EDS; Py-GC/MS

1. Introduction

1.1. Egyptian Artifacts in Portugal

Portugal houses an interesting collection of over 1000 Egyptian artifacts [1]. Three Egyptian collections stored in three Museums in Lisbon and Oporto were investigated.

In the *Museu Nacional de Arqueologia* (MNA) in Lisbon, a vast collection of Egyptian artifacts was acquired over the 19th and early 20th centuries. The collection includes the former King of Portugal's private collection, which was donated to the MNA by the state, after the royal family was overthrown [2]. As of today, the MNA has around 560 Egyptian artifacts, ranging from Prehistoric to the Coptic Periods. Among their collection, flint tools, pottery and stone vases, funerary relief sculptures, various funerary objects, and bronze objects can be found [2]. The museum has three human and seven animal mum-mies (a falcon, two ibis, and four crocodiles). While their provenances are unknown, the human mummies at some point belonged to aristocratic Portuguese families [3].

The Lisbon Mummy Project studied the mummies at the MNA, employing non-de-structive radiographic examinations of the specimens. It was done in partnership with *Imagens Médicas Integradas* (IMI) and with the support of Siemens Portugal [2,3].

The *Museu Arqueologico do Carmo* in Lisbon hosts an extremely diverse collection of objects collected towards the end of the 19th century and the first quarter of the 20th century including 1 Egyptian mummy with its sarcophagus. All objects are of unknown origin.

The *Museu de História Natural da Faculdade de Ciências da Universidade do Porto* (MHN-FCUP) in Oporto has a smaller collection of about 103 objects, ranging from the Predynastic period to the Byzantine Period [1]. It houses a wide array of artifacts including terracotta figurines, two funeral masks, two mummies and one sarcophagus [1,4]. The Egyptian artifacts stored at the MHN-FCUP were originally from the collection of the *Äegytisches Museum und Papyrussammlung* in Berlin, Germany [5]. It was offered to Portugal as a "gift", along with over 500 other artifacts from Melanesia, Ancient Greece, Turkey, Near East, China, Japan, Africa, and the Central and South Americas, when Portugal returned a collection of 448 boxes containing Assyrian artifacts [4,5]. The collection was found on board the *SS Cheruskia*, which, along with 69 other German and Austrian ships, had initially sought asylum in Lisbon from the British Royal Navy during the beginning of World War I but were eventually seized by Portuguese authorities after Germany declared war on Portugal in March 1916 [1,4,5].

1.2. The Egyptian Palette

Pigments and binders from the Egyptian period have been studied extensively. The earliest evidence of paintings in Ancient Egypt can be found in the predynastic period with walls of certain tombs elaborately decorated with designs in a range of colors. Similarly, painted fabrics such as leather and linen painted in reds, blues, greens, yellows, and blacks also serve as evidence of the deliberate use of pigments very early on in Egypt's history [6].

Pigments from this period were either natural pigments obtained from finely ground minerals or synthetic ones [6,7]. Egyptian pigments were mostly inorganic before the Roman Period [6] when the Romans introduced organic red lakes such as madder [8], which became commonly used in the production of pink paints and became a fashionable color choice for sarcophagi since that time period [9].

Ancient Egyptians produced many of their pigments such as the famous Egyptian blue and arsenic sulfides such as realgar (αAs_4S_4) and orpiment (As_2S_3) [10]. Historically, synthetic pigments begin to be used as early as the Dynastic Period [11]. Egyptian Blue ($CaCuSi_4O_{10}$) was first synthesized during the third millennium BC [12] by mixing a calcium salt (carbonate, sulfate, or hydroxide), a copper compound (ore or Cu-alloy scraps), and sand, and then heating to produce Egyptian Blue, which was then ground into a powder [6,13,14]. Organic sources of blue lake pigments were uncommon in ancient times and blue minerals such as Lapis Lazuli were rare [14]. Influence from the Greeks and the Romans during later periods introduced vermillion or cinnabar (αHgS), minium ($Pb^{2+}_2Pb^{4+}O_4$), and lead white ($2PbCO_3 \bullet Pb(OH)_2$) [11,15].

The typical stratigraphy of painted fragments on Egyptian artifacts was made up of one (or two when there is an overlapping in the motifs) paint layers applied on a preparatory layer acting as a substrate support. The preparatory layer was usually made of lime, gypsum, or an admixture of the two [7].

Pigments on Egyptian artifacts were typically applied using the tempera painting technique: the pigment was mixed with a water-soluble binding medium such as protein and polysaccharide-based materials [16,17] in order to achieve adhesion between the pigment grains. Examples of protein-based material that would have been available to the Egyptians are animal glue, eggs, and casein [16], whereas, as far as polysaccharide-based material is concerned, plant gum would have been readily accessible [17]. However, other types of binders such as natural resins, waxes, fats, and oil have also been identified on artifacts from Ancient Egypt [18].

The aim of the current study is twofold: (1) to conduct for the first time a diachronic multi-analytical study of pigments and binders used in funerary masks and sarcophagi

from two of the most important Egyptian Museum collections in Portugal with a time ranging from the Late Period until the Roman one, and (2) to assess whether any significant change in the used of painting materials could be identified within the same timeframe thus providing an overview of the development of these technologies over time and the potential influence of neighboring cultures.

The results of this study will contribute to the expanding database about Egyptian painting materials while, at the same time, helping in valorizing Egyptian collections in Portugal and highlighting the importance of a multidisciplinary approach in archaeometry also from an educational perspective [19].

2. Materials and Methods

2.1. Sampling

A total of 25 samples were analyzed from 5 artifacts: one funerary mask (Mask#1, see description below and Figure 1), from the *Museu Arqueologico do Carmo* in Lisbon; two funerary masks (Mask #2 and Mask #3 see description below and Figures 2 and 3) and one sarcophagus (Sarcophagus #2, see description below and Figure 4) from the Egyptian collection of the *Museu Nacional de Arqueologia* (MNA) in Lisbon and one sarcophagus (Sarcophagus #1, see description below and Figure 5) from the *Museu de História Natural da Faculdade de Ciências da Universidade do Porto* (MHN-FCUP) in Porto.

Figure 1. Funerary Mask #1 (photo credit Nick Schiavon).

Two of the artifacts (Mask #1 and Sarcophagus #1) had been previously studied at the *José de Figueiredo Laboratory* (LJF) in Lisbon in the 1980s where only stratigraphic analysis by OM were conducted on the pigmented layers while botanical and biological analysis were carried out to identify the type of wood used in the support and the presence of skin tissue attached to the mask [20,21]. In the case of Mask#1 and Sarcophagus#1, new samples were not taken directly from the artifacts themselves, but, instead, previously taken samples were subjected to complementary chemical and microscopic analysis by SEM+EDS, XRF, FT-IR, Raman Spectroscopy, and Py-GC-MS (see below for analytical operating conditions and specifications). Sampling was performed on the three other Egyptian funerary masks analyzed in this study. Samples were collected in areas that exhibited damaged or flaking-off painted layers. Sampling and analytical areas were chosen on the different colors representative of the areas subjected to micro-sampling. The average size of the samples was 0.5 cm in diameter.

Figure 2. Funerary Mask #2 (photo credits: HERCULES Laboratory).

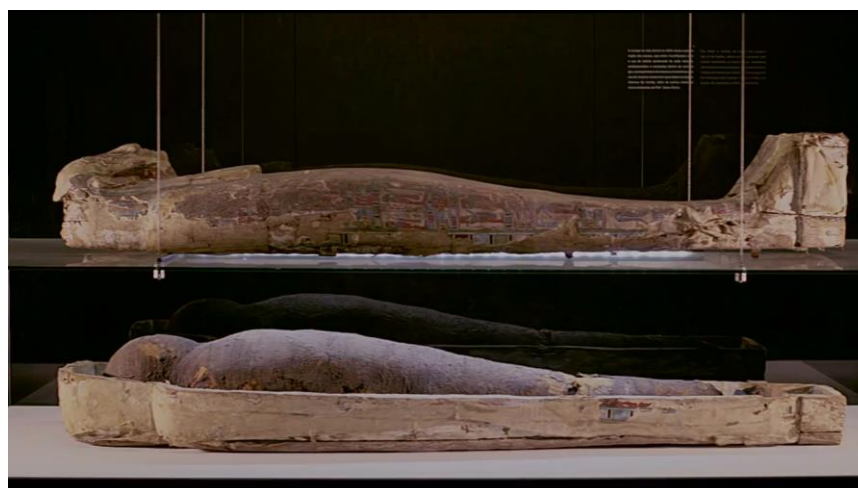**Figure 3.** Funerary Mask #3 (photo credits: IMI/MNA).

Figure 4. Sarcophagus #1 (photo credits: MHN-FCUP).

Figure 5. Sarcophagus #2 (photo credits: IMI/MNA).

2.1.1. Mask #1 (Archive Ref. LJF 1-80)

Funerary Mask LJF 1-80 (Figure 1) is a painted, cartonnage mask dated from the Late Period (c. VII–IV BC). It is believed to have belonged to Kawit, a priestess of Min [1]. Kawit's wooden sarcophagus was decorated with a representation of the Ouroboros, also known as the world serpent, which served as a preventive-magic motif that was common in the Late Period.

The mummy, itself, is reported to have been found in a terrible condition, with its head, upper, and lower limbs, and the embalmed internal organs missing. Restoration on the mask was performed in 1984 by the *José de Figueiredo Laboratory* in Lisbon.

2.1.2. Mask #2 (Archive Ref. MNA 228)

Funerary Mask MNA 228 (Figure 2) is also dated to the Late Period (c. VII–IV BC). The mask, placed on a wooden base, exhibits a lighter flesh color which is unusual for male masks. The eyes, eyebrows, beard, and wig are colored black. An interesting feature is a thin line that "connects" the beard to the face, almost emphasizing that it is a false beard [22].

2.1.3. Mask #3 (Archive Ref. MNA 226)

Funerary Mask MNA 226 (Figure 3) was made with pressed linen and resin and is dated to the Ptolemaic Period (c. IV–I BC). The flesh is painted in gold, with well-defined features with a red and black geometric necklace, adorning its neck.

2.1.4. Sarcophagus #1 (Archive Ref. LJF 1-89)

Sarcophagus LJF 1-89 from the MHN-FCUP (Figure 4) has been dated between the Late Period and the Graeco-Roman Period. It belongs to a young male mummy, estimated to have been 22–25 years old. The sarcophagus is elaborately painted with intricate

imagery related to the Egyptian belief about the afterlife. The "skin region" of the mask was painted using a reddish hue, a feature indicative of male sarcophagi/funerary.

2.1.5. Sarcophagus #2 (Archive Ref. MNA 216)

Sarcophagus MNA 216 (Figure 5) belongs to an unnamed individual and has been dated to the Ptolemaic Period (IV–I BC) [22,23]. The burial of the mummy was carried out using a standard procedure. It is adorned with a cartonnage mask and an elaborately painted shroud [3]. Supported by a base of linen and resin, its mask is gilded, specifically in the face region. It has a geometric necklace that has two crowned falcon heads on each end. The back of the wing has a winged deity with vertical hieroglyphics written on each side of the god [22]. The mummy had been previously analyzed as part of the Lisbon Mummy Project [3].

2.2. *Analytical Methodology*

Optical Microscopy (OM*)*. Unmounted samples were initially analyzed using the stereomicroscope, Leica M205 C. Polished cross sections were analyzed using the dark-field microscope, Leica DM 2500 M. OM was used to identify the layers present in the painted fragment samples. The layers in the cross sections were measured and the grains within each layer were then identified.

X-Ray Fluorescence Spectrometry (XRF*)*. In situ X-Ray Fluorescence Spectrometry (XRF) analysis for two of the masks at the MNA in Lisbon (Figure 6) was conducted, using a Bruker Tracer III SD handheld X-Ray Fluorescence Spectrometer. Analysis was made using a Ti/Al filter, 40 keV voltage, 11μA current, and 90s acquisition time. The instrument was fixed on a tripod and positioned close to the surface of the area of interest. Spectra were then analyzed using the software, ARTAX.

Figure 6. Masks undergoing XRF analysis at the MNA. (Photo credits: Sara Valadas).

Scanning Electron Microscopy-Energy-Dispersive X-Ray Spectroscopy (SEM-EDS*)*. Scanning Electron Microscopy-Energy Dispersive X-Ray Spectroscopy (SEM-EDS) was carried out using a Hitachi S-3700N variable pressure scanning electron microscope coupled with a Bruker XFlash 5010 Silicon Drift Detector Energy Dispersive X-Ray Spectrometer with the following operating conditions: accelerating voltage—20 keV; working distance—10.4 mm. Backscattered electron (BSE) detector mode was used.

Micro-Fourier Transform Infrared Spectroscopy (μFTIR). Samples were analyzed using micro-Fourier Transform Infrared Spectroscopy (μFTIR) using a Bruker Tensor 27 Mid-IR (MIR) spectrometer. The spectrometer coupled to the HYPERION 3000 microscope is controlled by the OPUS 7.2 software and has a MCT (Mercury Cadmium Telluride). The samples were analyzed in transmission mode using a 15× objective and an EX'Press 1.6 mm diamond compression microcell, STJ-0169. The IR spectra were plotted in the region of 400–6000 cm^{-1}, with 64 scans and 4 cm^{-1} spectral resolution.

Micro-Raman Spectroscopy (μ-Raman). Micro-Raman Spectroscopy was carried out using a XPlora Horiba Jobin Yvon Raman spectrometer coupled with an Olympus BX41

microscope. A 638 and 785 nm laser, with 10×, 50×, and 100× objective lenses was used with a 1% filter and an acquisition time ranging from 5–15 s, depending on the sample being analyzed. Spectra were compared with databases using the LabSpec 5 software.

Pyrolysis–Gas Chromatography/Mass Spectroscopy (Py-GC/MS). A system with a Frontier Lab PY-3030D double-shot pyrolyzer was used. The interface was maintained at a temperature of 280 °C. The pyrolizer was coupled to a Shimadzu GC2010 gas chromatographer, also coupled to a Shimadzu GCMS-QP2010 Plus mass spectrometer. A capillary column Phenomenex Zebron-ZB-5HT (30 m length, 0.25 mm internal diameter, 0.50 μm film thickness) was used for separation, with helium as a carrier gas, adjusted to a flow rate of 2.2 mL/min. The split-less injector operated at a temperature of 250 °C. GC temperature program was as follows: 40 °C during 5 min, ramp until 300 °C at 5 °C/min, and then an isothermal period of 3 min. The source temperature was placed at 240 °C, and the interface temperature was maintained at 280 °C. The mass spectrometer was programmed to acquire data between 40 and 850 m/z. The samples (<100 μg), previously derivatized with 3 μL of tetramethylammonium hydroxide (TMAH, 25% in methanol) in a 50-μL Ecocup capsule, were placed in the double-shot pyrolyzer using an Eco-stick. The capsule was placed in the pyrolysis furnace, and samples were pyrolyzed using a single-shot method at 500 °C.

3. Results and Discussion

3.1. Red and Yellow Pigments

Red pigments applied directly on top of the preparatory layer were found to be present in all the funerary objects investigated while only one sample from Sarcophagus #1 (sample D8) exhibited a yellow pigment.

Under SEM-EDS, the red pigments in Mask #1 appear to be composed by small, rounded pigment grains showing high concentrations of Fe (36.02 wt.%) and Ti (12.71 wt.%) with minor amounts of Ca, Si, and Al suggesting that the pigment is made up by a mixture of oxides (mainly iron oxides such as haematite-Fe_2O_3), aluminosilicate clays, and quartz (SiO_2) together with calcite. Such a composition is compatible with its identification as a red ochre [8].

μFTIR spectra of red pigmented areas showed the presence of bands corresponding to calcite, gypsum and kaolinite. In Figure 7, bands at 2510, 1794, 1420, 875, and 711 cm^{-1} correspond to calcite, with the last two bands referring to the asymmetric CO_3 bending [24]. Kaolinite was identified through the presence of the characteristic band at 3697 cm^{-1} due to O–H stretching frequencies associated with hydroxyl ions, while at 1082 and 1039 cm^{-1} the bands associated respectively with Si-O-Si and Si-O-Al bending are present. Quartz bands at 795 and 780 cm^{-1} are due to bending vibrational modes of Si-O-Si bonds. Gypsum was determined through the presence of vibration frequencies of sulfate groups at 1116 and 672 cm^{-1} and bands at 3526 and 1619 corresponding to the stretching frequencies of the O-H bonds [25]. Hematite and iron oxides were not detectable through FTIR, as these oxides are non-absorbing above 600 cm^{-1}, which makes assigning what type of ochre is present very difficult [26,27].
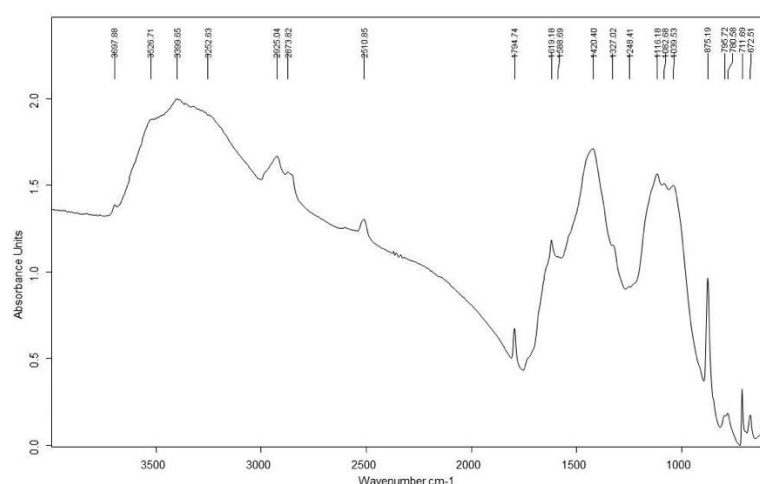
Figure 7. FTIR Spectrum for Mask #1, sample 1, red layer**.**

μRaman analysis on Mask #1 (Figure 8) confirms the EDS and μFTIR results, showing peaks at 413.8, 297.3, and 230.9 cm^{-1} [28,29] pertaining to hematite, the main mineral component of red ochres. However, because μFTIR gave evidence for the presence of quartz and clays, it is better to describe the pigment as a red ochre and not just as hematite [29]. Shifts in the spectra are expected when comparing the pure mineral and the mineral mixed with other materials such as clays or sand [30].

Figure 8. Raman Spectrum for Mask #1, sample 4, red layer**.**

EDS point analysis of the yellow pigments in sample D8 from Sarcophagus #1 displayed peaks for Fe, Ca, Si, Al, Mg, and Ti (9.92, 9.19, 9.14, 8.30, 2.06, and 1.65%, respectively) compatible with its interpretation as a yellow ochre [8].

Natural iron oxides deposits were commonly available in Egypt; moreover, their anhydrous and hydrated forms could be applied as pigments directly on the artifacts without the need for any specific pretreatment. Both ease of locally available supply and ease of use, therefore, explain be the reason behind the widespread presence of red and yellow ochres in the ancient Egyptian palette [10].

While in Mask #1 red ochre was the only pigment used for obtaining the red color, in other samples it has been found mixed with other red/orange red pigments. In red colored areas of Sarcophagus #1 for instance, SEM-EDS analysis shows small irregular pigment

grains homogeneously distributed within the pigmented layer which in the EDS spectra (Figure 9) display both As and S peaks with concentrations as high as 19.21 and 31.66 wt.%, respectively. This confirms the presence of realgar (αAs_4S_4), a red pigment commonly found in the Egyptian palette often in association with red ochre. Based on microscopic analysis, it does not appear that realgar and red ochre were used as individual pigments as there is no separation between areas rich in As and S versus those rich in Fe. Therefore, the red pigment in Sarcophagus #1 can be interpreted as having been obtained by mixing red ochre and realgar pigments.
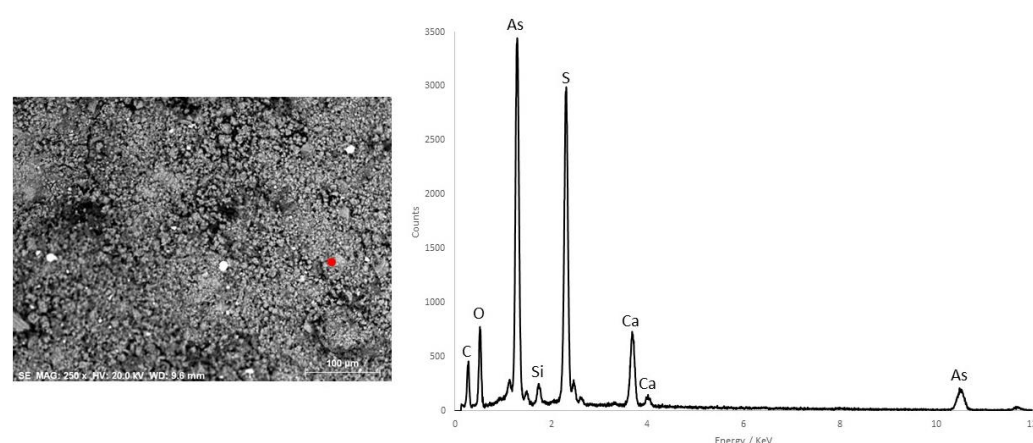

Figure 9. (**left**) Backscattered SEM image containing the point of analysis for Sarcophagus #1, sample D3, and (**right**) the corresponding EDS spectra of the analyzed spot.

The two funerary masks from the Ptolemaic period (Mask #3 and the cartonnage mask from Sarcophagus #2) contained cinnabar (HgS) as a main pigment together with small grains of red ochre found dispersed within the red layer.

Backscattered SEM imaging of red areas from the Ptolemaic funerary masks (Figure 10) shows in fact the presence of large and irregularly shaped pigment grains characterized by a higher BSEM image brightness as compared with surrounding grains. EDS point analysis on these grains show high concentrations of Hg (75.93 wt.%), along with S (and minor Ca) confirming the presence of cinnabar (HgS). In comparison, the EDS spectrum of surrounding grains show the presence of the Fe, Si, Al, K, Mg, and Ti peaks typical of red ochre.
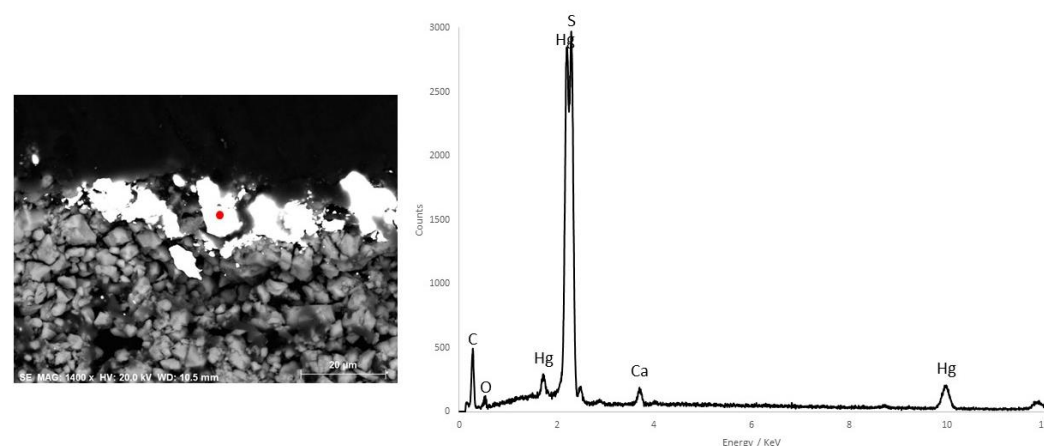

Figure 10. (left) Backscattered SEM image containing the point of analysis for Mask #3, sample M3-3, and (right) the corresponding EDS spectrum of the analyzed spot.

μRaman analysis of red colored areas from the Ptolemaic masks confirmed the SEM-EDS results by showing the presence of characteristic peaks of cinnabar at 343.5, 285.8,

and 253.1 cm⁻¹ [28]. In situ XRF results for Mask #3 yielded peaks for Ca, Hg, and Fe; further confirming the results that the red pigment used for the Ptolemaic funerary masks was, in fact, cinnabar.

The absence or presence of cinnabar in the decoration of Egyptian artifacts may indeed be used as a discriminating factor for dating their time of production (i.e., during or before the Graeco-Roman period) as the use of this pigment initiated in Egypt only as a result of political, cultural, and economic influences that occurred during and after the Graeco-Roman period [18,30,31]. In fact, while red ochres and realgar were used throughout most of the history of Ancient Egypt, the appearance of cinnabar as part of the Egyptian palette is evidence for the onset of external exchanges of not only commodities (as the Romans had control over HgS mines in Spain) but also of cultural assets during the Ptolemaic period [4]. This practice is confirmed in this study by SEM-EDS and Raman analyses showing the presence of cinnabar as red pigment only on the masks dated to the Ptolemaic period with its absence in earlier masks where, instead, red ochre and realgar were used as the main red pigments.

3.2. Pink Pigments

The pink pigments discussed in this study include pigments used for painting both bright pink as well as beige areas with a pink undertone. Pink and beige colored areas with a pink undertone were found in Sarcophagus #1 and Mask #1 samples. In the former, pink areas appear painted next to a light blue color and light-brown/beige areas with a pink undertone whereas in Mask #1 samples, for painting the "skin" areas of the masks.

Stratigraphic analysis of a Mask #1 sample (sample 5) shows a 20–38 μm thick layer characterized by light brown/beige grains intermixed with bright red and yellow grains. The EDS spectrum of this region shows a high concentration of Fe (41.80 wt.%), with smaller amounts of Ca, Si, Al, and Ti while its corresponding FTIR spectrum shows absorption bands pertaining to calcite and gypsum. As ochre has a color range varying from a light yellow to reds to dark browns [8], based on the color of the pigment grains, observed by OM, and the corresponding EDS results, the beige region most likely is composed of ochre, mostly towards brown hues, mixed with calcite and gypsum to achieve the flesh tones.

Like the red pigments found in Sarcophagus #1, also the pink pigmented areas are characterized by the presence of As and S EDS peaks with other areas showing mostly Fe peaks. Backscattered SEM analysis again suggests red ochre and realgar were intentionally mixed and not applied as two distinct separate layers. EDS spectra of pink areas show the highest concentration at 32.69 wt.%. Together with μFTIR results, which show calcite and gypsum peaks, the pink pigment most likely is composed by a mixture of red ochre, realgar, calcite, and gypsum.

Pink pigments mixed with red pigments and/or white pigments were extensively used in the decoration of Old and New Kingdom artifacts. This was before the introduction of organic red lakes such as madder, which became common during the Graeco-Roman period [18,31]. Despite the wide diachronic range covered by the artifacts investigated in the present study, however, no organic dyes were found of the pink colored areas of any of the samples.

3.3. Blue Pigments

All blue pigmented layers (Figure 11) appear to be heterogenous, showing the presence of blue angular crystals and transparent grains and, except for the blue pigment in Mask #1 (as discussed in the following section concerning black pigments), were applied as a single layer directly over the preparatory layer.
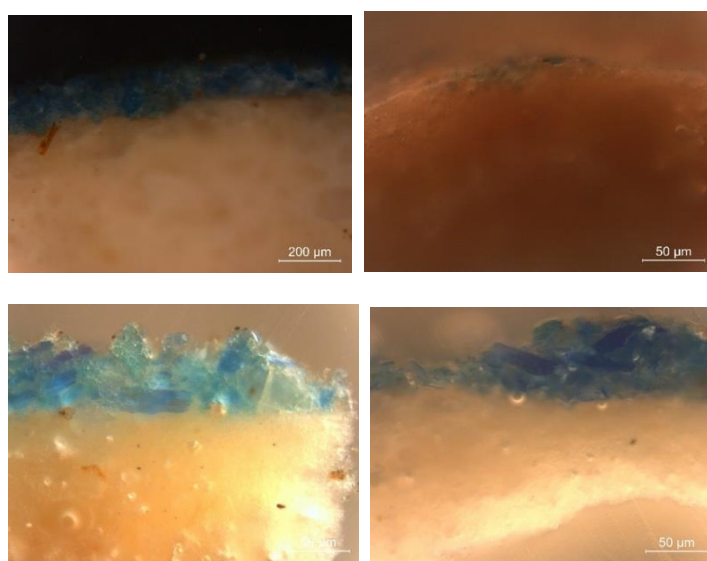
Figure 11. OM images for (**top left**) Sarcophagus #1, (**top right**) Mask #2, (**bottom left**) Sarcophagus #2, and (**bottom right**) Mask #3 showing blue pigmented single layers applied directly on preparatory substrate**.**

BSE investigation (Figure 12 left) confirms the heterogeneous nature of the blue pigmented layers as the angular crystals appear coarsely dispersed throughout the blue layer. EDS analysis (Figure 12 right) shows the angular blue crystals to be predominantly made up by Cu (9.40 wt.%), Ca (7.54 wt.%), and Si (19.84 wt.%). This suggests the presence of a Cu-silicate mineral, most probably cuprorivaite ($CaCuSi_4O_{10}$) which is one of the main components of Egyptian blue where is usually mixed with crystalline silica phases (SiO_2), alkali (Na), silica glass, and Cu oxides [32,33]. Cuprorivaite is a phyllosilicate composed of rings of SiO_4 tetrahedra linked by coordinated Cu^{2+} ions which are the ones responsible for the blue color [34–36]. Rounder grains mostly composed of Si are interpreted as the silica phase (SiO_2) typically formed in the production of Egyptian blue and present either as crystalline quartz or minor glass phase [37]. Minor peaks of Na and Cl were also present in blue colored areas of some samples particularly in association with Si-rich phases: the presence of Na (and the absence of K) could be explained by the use of natron as flux for the glass phase [37]. Taking into account that the presence of NaCl is known to produce an inhibiting effect in the process of production of Egyptian blue [38], the presence of chlorides could be regarded as evidence for degradation of the Egyptian blue as the detection of Cu-chlorides such as atacamite seems to confirm (see also green pigment section below).
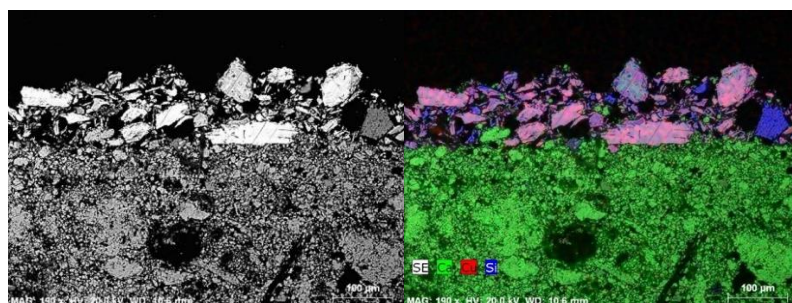

Figure 12. Backscattered SEM (**left**) of the cross-section of Sarcophagus #2, sample M2-2, at 190× magnification and (**right**) corresponding EDS elemental map (Ca, Cu, Si)**.**

μFTIR results yielded spectra for all the blue pigments that exhibited bands corresponding to cuprorivaite, gypsum, calcite, and calcium oxalate. The peaks within the range of 1280 to 1000 cm^{-1} are characteristic for Egyptian Blue (cuprorivaite), caused by

the Si-O-Si anti-symmetrical stretching vibrations [7,27,37]. Figure 13 shows peaks in this region at 1160, 1058, and 1010 cm⁻¹. While peaks at 793, 755, and 666 cm⁻¹ refer to symmetrical Si-O-Si stretching [37]. Gypsum bands were identified at 3529, 3406, 3242, 1681, and 1620 cm⁻¹. On the other hand, calcite peaks in the spectrum were located at 1796 and 883 cm⁻¹. Peaks in the 2900 cm⁻¹ region possibly refer to calcium oxalate [25].
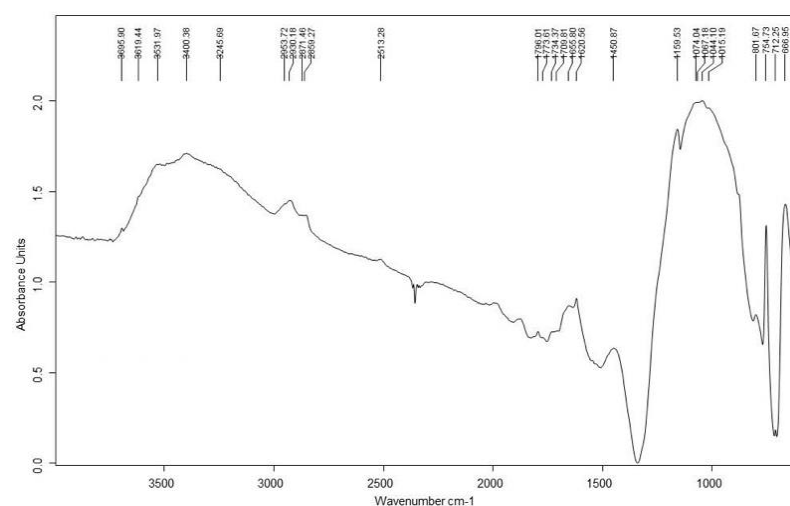

Figure 13. FTIR Spectrum for Sarcophagus #1, sample D4, blue layer**.**

Blue portions of Mask #2 and Mask #3 were also analyzed by in-situ XRF. The XRF spectra for the masks show peaks for Cu, Ca, and Fe, confirming the SEM-EDS and μFTIR results.

All Egyptian Blue samples analyzed, despite the difference in time period, show similar compositions with the exception of Sarcophagus #1 samples (Figure 14), where the presence of Sn reached concentrations as high as 55.74 wt.%.
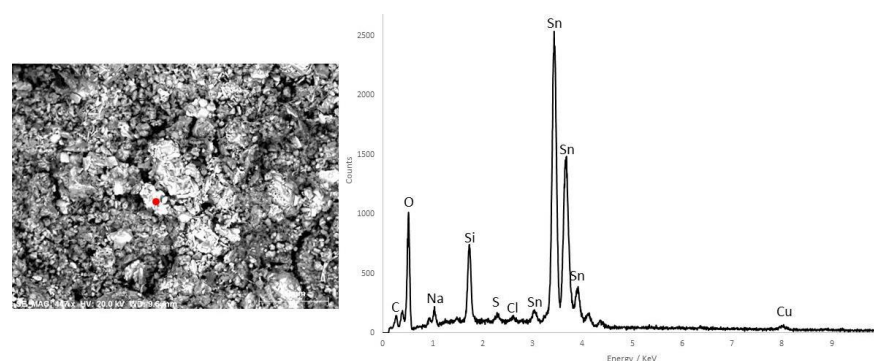

Figure 14. (**left**) Backscattered SEM image containing the point of analysis for Sarcophagus #1, sample D4, and (**right**) the corresponding EDS spectrum of the point analyzed.

No Cu ore known to have been exploited during Egyptian times for the production of Egyptian blue could explain such high values of Sn; however, production of copper-based pigments was not necessarily always associated with ores containing Cu-minerals such as malachite. The addition to the melt of recycled scraps of fillings of metallic Cu or Cu alloys such as bronzes has been suggested by many authors [36,37]. The blue was produced by melting starting mixtures of SiO_2-rich sand, bronze scrap, Na- and K-bearing fluxes together with lime. When copper–tin alloy filings (bronze) were used as a copper source, copper reacted with calcium and silica to form cuprorivaite, and the remaining tin crystallized as tin oxide [36,37].

Therefore, it is not uncommon to find Sn and Pb in some Egyptian blue samples, as these metals were typically alloyed with Cu to make bronzes. The presence of Sn and trace amounts of As and Pb has been proposed as evidence for a correlation between the production of Egyptian Blue and the development of Cu alloys in Egypt. The emergence of Sn, As, and Pb in Egyptian Blue in later dynasties coincides with the increasing development of the technology of production of Cu bronzes causing bronze artifacts to become sufficiently common as to offer the option of being recycled for Egyptian blue pigment production [39].

3.4. Green Pigments

Blue and green pigments are not distinguishable by EDS elemental analysis as both are primarily Cu-containing pigments, the distinguishing features being the ratios Cu-oxide/bulk lime (higher in Egyptian blue) and silica/bulk lime (higher in green pigments) [30,36]. As the lime contents of Egyptian blue and green frit can overlap, it has been suggested that the difference in production was obtained by reducing the amount of Cu from the recipe [40].

Sarcophagus#1 was the only sample to display green pigments. Two fragments were analyzed from the sarcophagus: D3, which is only green, and D8, which is a multicolored sample, containing other colors such as blue, red, and yellow.

Under OM, the surface of D3, which is primarily green, has multiple colors and not only a singular hue of green. The surface appears to be heterogenous in coloring with blues, blacks, and whites present throughout.

BSE investigation further confirms the heterogeneity of the green layer in sample D3. EDS point analysis for one area shows high concentrations of Cu (29.72 wt.%), Ca (8.22 wt.%), and Si (3.61 wt.%), which is similar to the results obtained in Egyptian Blue samples. Like blue pigments, the chromophores responsible for the green color are Cu^{2+} ions. EDS point analysis (Figure 15) on another grain gives a very different spectrum. Sn (35.35 wt.%) is present and has a significantly higher value than Cu, Si, Ca (3.66, 6.67, 7.91 wt.%). The presence of high % of Sn in pigments from the Sarcophagus #1 is again worth noting. As discussed in the previous section, Sarcophagus #1 was the only artifact showing pigments (in that case Egyptian blue) enriched in Sn; the same pattern is now repeated in the analysis of green pigments from the same artifact. As the technique for the production of green frit [40,41] is similar to the one for Egyptian Blue, with only minor changes in the ratios of its components and the temperature in the kiln, this would mean that recycled Cu bronze scraps may have been the source of the copper used also for the production of the green pigments.
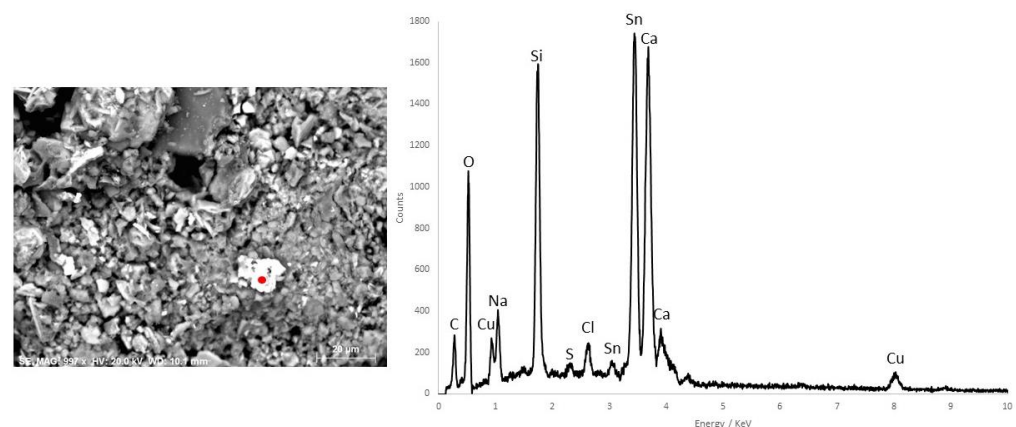

Figure 15. (left) Backscattered SEM image showing the point of analysis for Sarcophagus #1 (sample D3) and (**right**) the corresponding EDS spectra of the point analyzed.

The results for μFTIR for the green pigments show the presence of Egyptian Blue, atacamite, paratacamite, and kaolinite. The FTIR spectra for Egyptian green would be similar to that of Egyptian blue, although with stronger silicate bands [37]. Being both silicate-based pigments, they show peaks characteristic of Si-O stretching from 1100–800 cm^{-1} [27]. The FTIR spectrum for Mask #1 (sample D3) (Figure 16) exhibits peaks at 780 and 665 cm^{-1}, which are peaks characteristic for Si-O-Si bending in Egyptian Blue. Absorption bands for calcite are present at 1794 and 1449 cm^{-1}. Kaolinite bands were observed at 1050 and 1009 cm^{-1}, while gypsum bands are at 1619 and 1159 cm^{-1} [25]. Differentiating themselves from the FTIR spectra obtained for the Egyptian Blue, absorption bands of atacamite and paratacamite were observed in all green pigments. This can be seen in Figure 16, where 3446 and 3337 cm^{-1} are representative of these Cu chlorides [42,43], thus explaining the presence of Cl in the EDS spectra of the green samples.
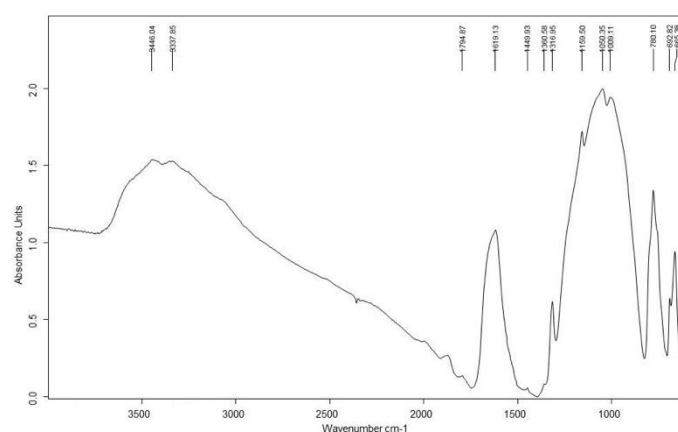

Figure 16. FTIR Spectrum for sample D3 of Sarcophagus#1, green layer**.**

The presence of atacamite and paratacamite from the μFTIR results, the occurrence of blue grains upon OM inspection of the surface of the green paint fragment analyzed, and the fact that both blue and green samples from Mask #1 are the only samples with Sn present can lead to the interpretation of the green pigment merely as a degradation product of Egyptian Blue. However, because Egyptian green is also a Cu-based pigment, it can also degrade into atacamite or paratacamite [43,44]. This means that the mere presence of atacamite and paratacamite in the green pigments of Sarcophagus #1 cannot help in assessing whether the original pigment was blue or green.

Figure 17 shows EDS map of Mask #1 sample D8, the multicolored sample. The highlighted area contains green, yellow, and blue on its surface with black visible underneath the blue and green layers. While there is a certain amount of both Si and Cu dispersed throughout the surface of the fragment, there is a clear division between the green paint and the blue paint. The green paint exhibits higher concentrations of Cu while the area painted in blue paint is high in Si. In the map, it can be seen that these are two separate areas that do not necessarily overlap. This could mean that most probably the green pigment in Sarcophagus #1 is, in fact, intentional, and not merely a degradation of Egyptian Blue.

Like in the cross section, the green paint layer observed in Sarcophagus #1 sample D8 did not show any elemental peak in the EDS analysis that could suggest a yellow pigment mixed with Egyptian blue. Despite it being next to a region of yellow paint, the EDS spectrum for this region does not show elements corresponding to yellow ochre, which was the pigment identified.
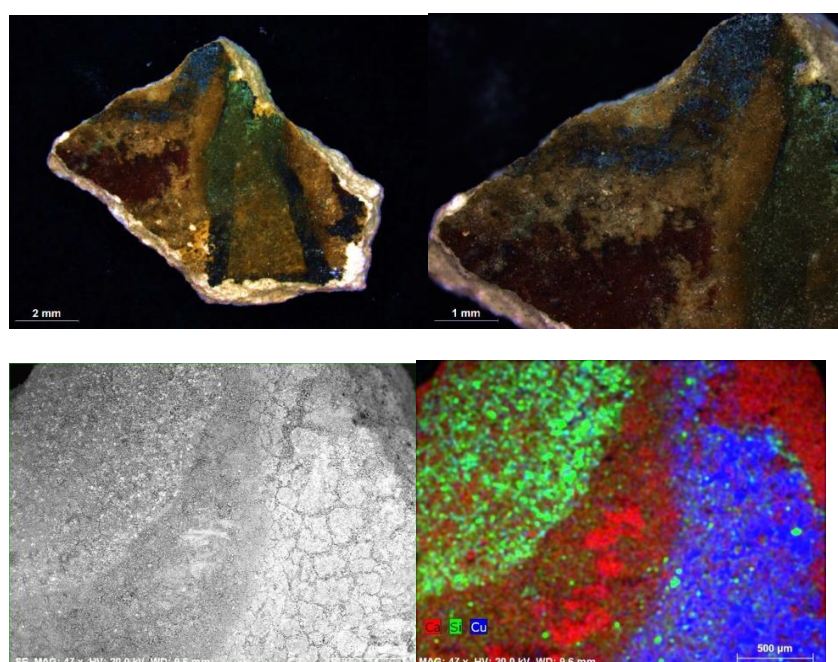
Figure 17. (**top**) OM image of the Mask #1, sample D8, at 10× and 100× magnification; (**bottom**) backscattered SEM image; and EDS map of the same area of interest (Ca, Cu and Si). See text for explanation**.**

3.5. Purple Pigments vs. Black Pigments

Two of the black paint fragments analyzed from two masks: Mask #1 and Mask #2, displayed very interesting results. Upon visual inspection, they appeared black in color but, under OM, they reveal to be composed by a mixture of red and blue pigments sometimes also showing some layering (in Mask #2 in particular; Figure 18).

Usually when blue is mixed with red, purple is produced. However, according to studies on the Egyptian palette, true purple does not seem to be found other than in Predynastic pottery [6,31].
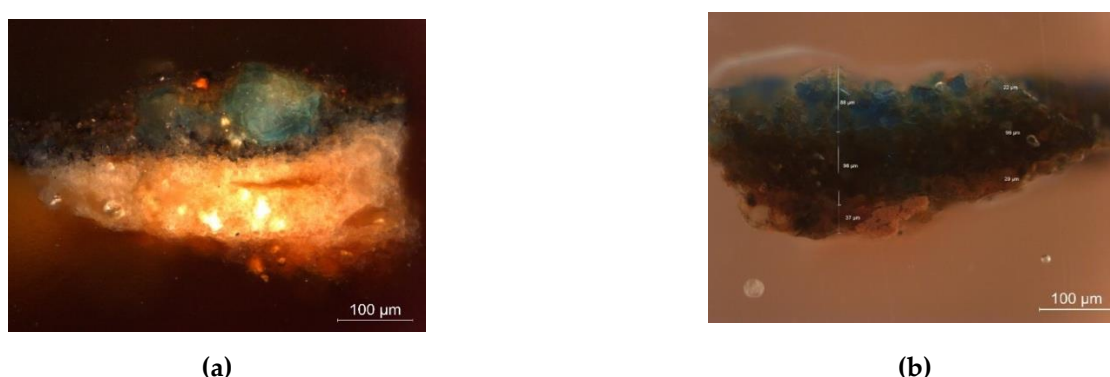

(a)   **(b)**

Figure 18. OM images for the cross-section of (**a**) Mask #1, sample 7, and (**b**) Mask #2, sample M1-1**.**

EDS point and map analysis (Figure 19) on individual grains on both samples give a clear distinction between blue grains, showing predominantly Cu, Si, and Ca peaks typical of Egyptian blue and red colored grains with high concentrations of Fe and Ti, typical of red ochre.
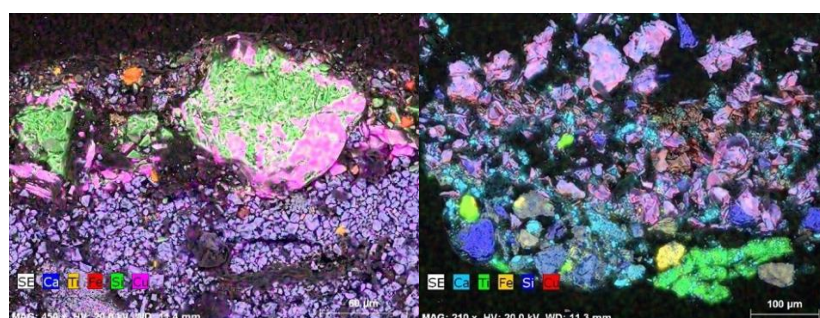
Figure 19. EDS Mapping (Ca, Ti, Fe, Si, and Cu) of (**left**) Mask #1 sample 7 and (**right**) Mask #2 at the region where the mixing of blue and red pigments was observed**.**

Deep red-orange grains (mainly red ochre) have been observed in some layers of Egyptian blue collected from a Ptolemaic temple of Hathor in Thebes [7]. In this study, it was suggested that red ochre was added on purpose to the blue pigment to produce special hues because Egyptian blue is transparent, meaning it is easily subject to color modification. Although not exactly a similar situation, some artifacts were found to be painted with a mixture of Egyptian blue and a brownish binder, producing an almost black pigment when mixed with darker types of Egyptian blue, or a brown-green color when mixed with lighter colored ones [45].

Similarly, in situ XRF (Figure 20) conducted on the beard region of Mask #2 identified the presence of Cu and Fe, which would pertain to Egyptian blue and red ochre.

Samples were taken from the hair portion of the funerary masks. For Mask #2, specifically, a sample was taken from the beard of the mask. Under visual, macroscopical examination, both samples appear to have a blackish color, ranging between very dark brown to black with a bluish hue. This could mean that an admixture of the two pigments were used to achieve a certain, specific hue or shade of a very dark purple color hitherto not found in the Egyptian palette, or something closer to a brown/black color.
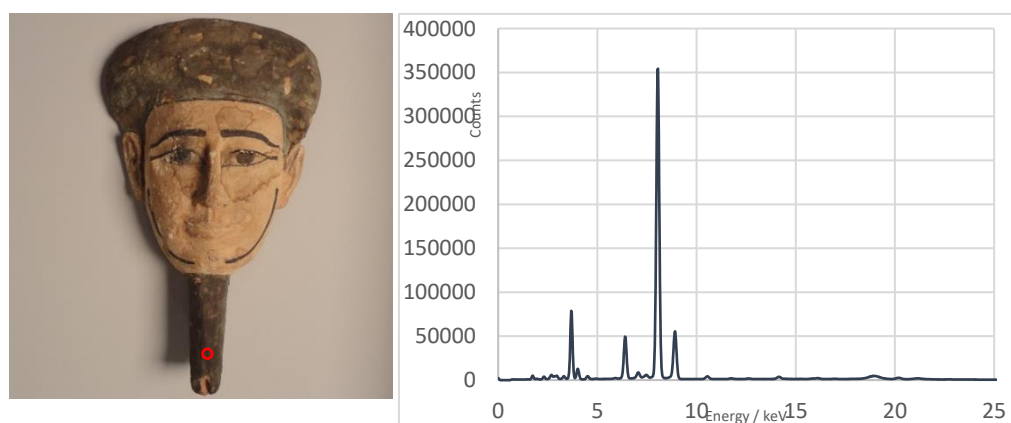

Figure 20. Mask #2 with area of interest, subjected to XRF analysis encircled in red (black beard) and corresponding XRF spectrum (left)**.**

3.6. Preparatory Layer

Chalk was identified to be the preparatory layer for all the funerary artifacts analyzed, composed primarily of calcite with coccoliths dispersed within the material.

Stratigraphic analysis of the pigment cross sections shows that most paint layers, (2 or 3 depending on the investigated area) had been applied directly on the preparatory layer. As the samples were mostly collected from heavily damaged areas, the stratigraphy of the sample did not include the substrate (cartonnage or base of the mask or sarcophagus) and, therefore, the thickness of the preparatory layer cannot be determined.

SEM imaging shows the widespread presence in the preparatory layer of coccoliths (Figure 21), marine calcareous microfossils that can be found as main constituents of micritic limestones [46]. EDS chemical analysis for the preparatory layer of all samples confirms the presence of Ca, C, and O peaks of calcite ($CaCO_3$).
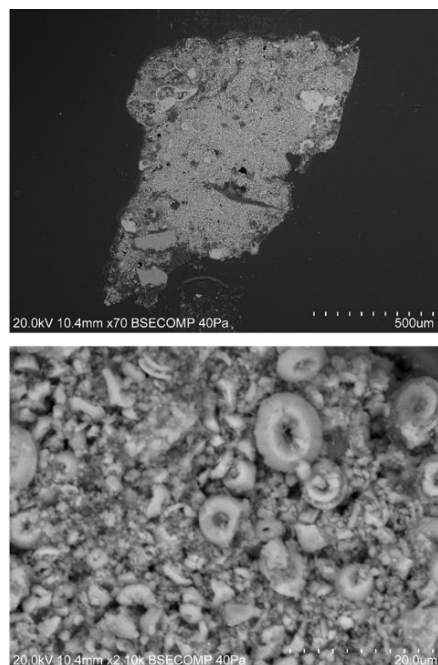

Figure 21. Backscattered SEM image of a sample taken from Mask #3 showing chalk nature of the preparatory layer**.**

μFTIR analysis yielded a spectrum similar to the reference library spectra for calcite, particularly at bands around 2510, 1795, 1436, 877, and 712 cm^{-1}. The peaks at 877 and 712 cm^{-1} relate to the antisymmetric bending, while 2510 and 1795 cm^{-1} are combination bands for calcite [24,38]. Peaks at 848.29 and 782.97 cm^{-1} could be due to trace amounts of quartz. The presence of quartz is not unexpected, as sand was added to the ground layer in order to improve its workability [15].

Raman spectrum obtained for the preparatory layers gives an absorption band at around 1087 cm^{-1}, which is characteristic for calcite [43], corroborating the other data collected.

3.7. Binders

According to literature, different types of binding media have been used in Ancient Egypt. While several researchers cite tempera-based techniques as the main method used in the application of paints [16,17], proteinaceous and polysaccharide-based materials, waxes, fats, and oils have also been reported in Ancient Egyptian artifacts [18].

An organic layer, found in between the pigment and the preparatory layer, from Mask #1, sample D3, was isolated for FTIR analysis. This was the only sample where an organic layer was observed. The μFTIR spectrum for the organic layer showed peaks belonging to a proteinaceous material, wax, and calcite. Absorption bands for proteins found were 3386, 3290, 3064, 1636, 1514, and 1387 cm^{-1}. Amide groups have very characteristic vibrational modes that allow it to be distinguished from other organic material [16]. 3386 and 3290 cm^{-1} refer to the O-H stretching and N-H stretching, respectively, while 3064 cm^{-1} is assigned an Amide II overtone [47–49]. 1636 cm^{-1} is attributed to Amide I, specifically caused by C=O vibrations [16]. Amide II is responsible for the absorption band at 1514 cm^{-1}, due to the protein deformation (in-plane bending) of NH_2 [16,48]. Amide III

was assigned to the peak at 1387, due to C-N stretching and N-H bending [16]. Wax was assigned through the presence of two sharp twin peaks at 2917 and 2849 cm^{-1}.

At a different point, the FTIR spectrum showed wax peaks appear more predominant than protein peaks. 2917 and 2849 cm^{-1} would refer to the νCH$_2$ and CH$_2$ stretching, respectively [48]. Trace amounts of calcite were determined through absorption bands at 1444, 877, and 718 cm^{-1} [24]. There are also several smaller peaks that are characteristic of proteinaceous material, which are not so easily assigned. These peaks are found between 1400–1316 and 1266–700 cm^{-1} regions, which pertain to the absorption bands from the vibrations of amino acid side chains [16,48].

FTIR results for the preparatory layer for Mask #2 show absorption bands that could be related to proteinaceous materials. Peaks were observed at 1680, 1539, and 1416 cm^{-1}, pertaining to the amide bonds.

Peaks attributable to organic compounds were observed in the FTIR spectra for Sarcophagus #2 and Mask #3. The paint layers exhibited a strong absorption band in the 1700 cm^{-1} region that can be attributed to some organic compound, possibly the binder used. The 1750–1700 cm^{-1} is attributed to the C=O (ester) stretching region, which is present in resinous material, waxes, and even proteins [16,48,49].

While the presence of proteinaceous materials and waxes was confirmed through μFTIR, the exact type of protein material or wax used as binding media was not determined.

To allow a better identification of the organic markers in the binders, Pyrolysis Gas Chromatography Mass Spectroscopy (Py-GC/MS) analyses were performed as a complementary analytical technique [48,50–52]. For this study, an innovative methodology to Py-GC/MS data interpretation using expert knowledge integrated into a Microsoft Excel workbook was selected—ESCAPE: Expert System for Characterization using AMDIS Plus Excel. This system was created by researchers at the Getty Conservation Institute and conservators at the J. Paul Getty Museum and involves the development of an expert system to simplify the identification of materials in Py-GC/MS data [53] using AMDIS, a freeware program developed by the National Institute of Standards and Technology (NIST) that systematizes the process of identifying compounds in GC/MS sample data files by means of mass spectral library searching.

Py-GC/MS was conducted on samples from the two sarcophagi. Micro-sampling was used to get results from the different paint layers. For Sarcophagus #1/Sarcophagus #2, a green/brown paint layer and respective preparatory layers were analyzed (total of 4 samples).

Abietic and pimaric acid derivatives were detected in Sarcophagus #1 green paint layer and Sarcophagus #2 brown paint and preparatory layers, pointing to the presence of a *Pinaceae* resin. Beeswax was also identified in brown paint layer in Sarcophagus #2, based on the detection of characteristic beeswax biomarker 15-methoxy palmitic acid methyl ester and lignoceric acid. *n*-alkanes showed a simple distribution on the samples' pyrogram (data not shown), mainly odd-numbered, but the presence of even-numbered *n*-alkanes might be the result of adding paraffin to the beeswax.

Protein identification in the ESCAPE workbook involves reviewing tables of marker compounds and considering their total peak area in the sample. Confidence in the identification results is greater when multiple marker compounds for a particular material are detected. For example, experience has demonstrated that identification of an egg binder or animal glue in a sample can be straightforward because multiple markers are formed by these materials [53]. Analysis of the pyrogram from the green paint layer from Sarcophagus #1, exhibited only a few non-specific protein biomarkers, which is not enough to establish an origin for the protein binder. Concerning the green layer preparatory sample, several biomarkers related to the presence of protein in reference materials, L-proline, hydroxyproline, and other biomarkers that are found in egg white reference materials were detected (data not shown). Identification was done by using correlation coefficients to find closest matching reference materials, with the help of the ESCAPE expert system.

The different compounds identified reflected the composition of egg white as binding media. Palmitic to stearic acids ratio (P/S) registered a value of 2.89, which is also compatible with the presence of an egg binder.

To summarize, Sarcophagus #1 results show the presence of protein binders in both the green paint layer and its preparatory layer, very likely an egg binder (egg white). Sarcophagus #2 results show the presence of *Pinaceae* resin in the preparatory layer, while a mixture of beeswax and the *Pinaceae* resin was observed in the brown paint layer. Chemical analyses of Late Roman-Egyptian adhesives showed similar results [51]. The use of these adhesives has been documented in Ancient Egyptian times, both separately and as mixtures.

4. Conclusions

The aim of this study was to characterize materials from Egyptian funerary masks and sarcophagi found in the *Museu Nacional de Arqueologia* and the *Museu Arqueologico do Carmo* in Lisbon and the *Museu de História da Faculdade de Ciêncas da Universidade do Porto* in Porto that range from the Late Period to the Roman Period. Through a multi-analytical approach, techniques such as OM, SEM, µFTIR, µRaman, Py-GC/MS, and XRF supplied information on the type of materials found in the samples studied (see summary in Table 1).

There appeared to be a mostly uniform color palette for the funerary artifacts over the 1000-year period of the materials studied. The pigments found used were mostly inorganics—red ochres, realgar, Egyptian blues and greens, which are in accordance with the established Ancient Egyptian palette [6,31,33]. Similarly, the preparatory layer of chalk, consisting of calcite, coccoliths microfossils and gypsum, remains unchanged over time.

One significant change over time is the introduction of cinnabar as a main red pigment in the Ptolemaic artifacts, Sarcophagus #2 and Mask #3, alongside red ochres, which was more common in previous dynasties. This is in accordance with historical accounts, as the use of this pigment appears in Egyptian history through the influence of the classical world during the Graeco-Roman Period [28].

Egyptian blue was found to be the main pigment in the blue layers analyzed for all the funerary objects investigated in this study. However, the presence of Sn in Sarcophagus#1 seems to suggest that the Cu-source used to make this Egyptian blue was recycled bronze. Similarly, the green pigments used in the same sarcophagus show high concentrations of Sn, indicating that it was most likely sourced from similar material. The absence of Sn in the other samples suggest that the Cu-source for these pigments came from a Cu ore such as malachite.

The black pigments for Mask #1 and Mask #2, which are both Late Period masks, were found not to be composed by a carbon-based pigment, which is typical of the Egyptian palette, but, instead by a mixture of Egyptian blue and red ochre, suggesting the possibility of purple pigments. However, extensive literature on the Egyptian palette does not have any mention of the use of purple pigments in Ancient Egyptian art [6,29]. As both pigments were taken from the 'hair' regions of the funerary masks, the mixture of the two pigments could possibly be intentional in the creation of a specific hue or tone to emulate dark hair coloring.

Overall, the project has gained useful information about the Egyptian funerary masks and sarcophagi housed at the MNA, MAC and MHN-FCUP in Portugal, adding to the database of Ancient Egyptian painting materials and valorizing these Egyptian collections in Portugal.

Table 1. Analytical results: summary.

Funerary Mask #1 Late Period	4	Red	-	Calcite, gypsum, quartz, kaolinite	Haematite	C, O, Fe, Ti, Ca, Si	Red Ochre	Chalk
	5	Beige	-	Calcite, gypsum, quartz, kaolinite	-	C, O, Fe, Ti, Ca, Si, Al, K, Mg	Red Ochre + Calcite	
	7	Black	-	EB, calcite, gypsum, calcium oxalate	-	C, O, Si, Ca, Cu (EB)	Egyptian Blue + Red Ochre	
Sarcophagus #1 Late Period – Roman Period	D3	Green	-	-	-			Chalk
	D4	Blue	-	EB, calcite, gypsum, calcium oxalate	-	O, C, Si, Ca, Sn, Na, Cu, Cl (EB)	Egyptian Blue	
		Pink	-	Calcite, gypsum, quartz, kaolinite, calcium oxalate	-	O, C, S, As, Ca, Si, Fe	Red Ochre + Realgar + Calcite + Gypsum	
	D8	Red	-	Calcite, gypsum, quartz, kaolinite, calcium oxalate	-	O, C, S, As, Ca, Si, Fe	Red Ochre + Realgar	
		Blue	-	EB, calcite, gypsum, calcium oxalate	-	O, C, Si, Ca, Sn, Na, Cu, Cl (EB)	Egyptian Blue	
		Green	-	-	-	-	Egyptian Green	
		Yellow	-	-	-	-	Yellow Ochre	
Funerary Mask #2 Late Period	M1-1	Black	-	-	-	-	Egyptian Blue + Red Ochre	Chalk
	M1-3	Blue	Cu, Ca, Fe	EB, calcite, gypsum	-	C, O, Si, Ca, Cu (EB)	Egyptian Blue	

Sarcophagus #2 Ptolemaic Period	M2-2	Blue	-	-	-	C, O, Si, Ca, Cu (EB)	Egyptian Blue	Chalk
	M2-3	Red	-	Calcite, gypsum	Cinnabar	-	Cinnabar + Red Ochre	
Funerary Mask #1 Ptolemaic Period	M3-1	Blue	Cu, Ca, Fe	EB, calcite, gypsum	-	-	Egyptian Blue	Chalk
	M3-3	Red	Hg, Ca, Fe	Calcite, gypsum	Cinnabar	-	Cinnabar + Red Ochre	

References

1. Araújo, L.M.D. *A Coleção Egípcia do Museu de História Natural da Universidade do Porto*; Universidade do Porto: Porto, Portugal, 2011; p. 272.
2. Figueiredo, A. The Lisbon Mummy Project: The employment of Non-Destructive Methods in Mummy Studies. 2011. Available online: http://www.mnarqueologia-ipmuseus.pt/documentos) (accessed on 08-09-2017).
3. Prates, C.; Oliveira, C.; Sousa, S.; Ikram, S. A kidney's ingenious path to trimillenar preservation: Renal Tuburculosis in an Egyptian mummy? *Int. J. Paleopathol.* **2015**, *11*, 7–11.
4. Veiga, P. 'A Rescue from Oblivion'. In *Collections at Risk: New Challenges in a New Environment*; Derriks, C., Ed.; Lockwood Press: Atlanta, GA, USA, 2017; pp. 131–137.
5. Afonso, M.G. A Coleção Egípcia da Universidade Do Porto—Histórias da sua Aquisição. 2015. Available online: https://www.academia.edu/22550552/A_COLEÇÃO_EGÍPCIA_DA_UNIVERSIDADE_DO_PORTO_HISTÓ-RIAS_DA_SUA_AQUISIÇÃO) (accessed on on 08-09-2017).
6. Lucas, A.; Harris, J.R. *Ancient Egyptian Materials and Industries*, 4th ed.; Edward Arnold: London, UK, 2012.
7. Marey Mahmoud, H.H. Microanalysis of blue pigments from a Ptolemaic temple of Hathor (Thebes), Upper Egypt: A case study. *Surf. Interface Anal.* **2012**, *44*, 1271–1278.
8. Elias, M.; Chartier, C.; Prévot, G.; Garay, H.; Vigaud, C. The colour of ochres explained by their composition. *Mat. Sci. Eng.* **2006**, *B127*, 70–80.
9. Scott, D.; Dennis, M.; Khandekar, N.; Keeney, J.; Carson, D.; Swartz Todd, L. An Egyptian cartonnage of the Graeco-Roman period. *Stud. Conserv.* **2003**, *48*, 41–56.
10. Uda, M.; Sassa, S.; Yoshimura, S.; Kondo, J.; Nakamura, M.; Ban, Y.; Adachi, H. Yellow, red and blue pigments from ancient Egyptian palace painted walls. *Nucl. Instrum. Methods Phys. Res. B* **2000**, *163*, 758–761.
11. Di Stefano, L.M.; Fuchs, R. Characterisation of pigments from Ptolemaic Egpytian *Book of the Dead* papyrus. *Archaeol. Anthr. Sci.* **2011**, *3*, 229–244.
12. Mazzocchin, G.A.; Rudello, D.; Bragato, C.; Agnoli, F. A short note on Egyptian blue. *J. Cult. Herit.* **2004**, *5*, 129–133.
13. Barnett, J.R.; Miller, S.; Pearce, E. Colour and art: A brief history of pigments. *Opt. Laser Technol.* **2006**, *38*, 445–453.
14. Berke, H. Chemistry in Ancient Times: The Development of Blue and Purple Pigments. *Angew. Chem. Int. Ed.* **2002**, *41*, 2483–2487.
15. Scott, D.; Warmlander, S.; Mazurek, J.; Quirke, S. Examination of some pigments, grounds and media from Egyptian cartonnage fragments in the Petrie Museum, University College London. *J. Archaeol. Sci.* **2009**, *36*, 923–932.

16. Duce, C.; Ghezzi, L.; Onor, M.; Bonaduce, I.; Colombini, M.P.; Tine, M.R.; Bramanti, E. Physico-chemical characterization of protein-pigment interactions in tempera pain reconstructions: Casein/cinnabar and albumin/cinnabar. *Anal. Bioanal. Chem.* **2012**, *402*, 2183–2193.

17. Granzotto, C.; Arslanoglu, J. Revealing the binding medium of the Roman Egyptian painted mummy shroud. *J. Cult. Herit.* **2017**, *27*, 170–174.

18. Scott, D. A review of ancient Egyptian pigments and cosmetics. *Stud. Conserv.* **2016**, *61*, 185–202.

19. Festa, G.; Saladino, M.L.; Mollica Nardo, V.; Armetta, F.; Renda, V.; Nasillo, G.; Pitonzo, R.; Spinella, A.; Borla, M.; Ferraris, E.; et al. Identifying the Unknown Content of an Ancient Egyptian Sealed Alabaster Vase from Kha and Merit's Tomb Using Multiple Techniques and Multicomponent Sample Analysis in an Interdisciplinary Applied Chemistry Course. *J. Chem. Educ.* **2021**, *98*, 461–468, doi:10.1021/acs.jchemed.0c00386.

20. Ribeiro, I.; Esteves, L. *LJF 1-80 Unpublished Report*; José de Figueiredo Laboratory:Lisbon 1980.

21. Ribeiro, I.; Esteves, L. *LJF 1-89 Unpublished Report*; José de Figueiredo Laboratory: Lisbon, 1989.

22. Araújo, L.M.D. *Antiguidades Egípcias*; Museu Nacional de Arqueologia: Lisboa, Portugal; Instituto Português de Museus: Lisboa, Portugal, 1993; Volume 1, p. 406.

23. Figueiredo, A.; Owens, L.S.; Oswald, R. Egyptian mummies at the Museu Nacional de Arquelogia, Lisbon: A proposed program of study. *Pap. Inst. Archaeol.* **2011**, *13*, 101–105.

24. Bracci, S.; Caruso, O.; Galeotti, M.; Iannaccone, R.; Magrini, D.; Picchi, D.; Pinna, D.; Porcinai, S. Multidisciplinary approach for the study of an Egyptian coffin (late 22nd/early 25th dynasty): Combining imaging and spectroscopic techniques. *Spectrochim. Acta Part A Mol. Biomol. Spectrosc.* **2015**, *145*, 511–522, doi.org/10.1016/j.saa.2015.02.052.

25. Genestar, C.; Pons, C. Earth pigments in paintings: Characterisation and differentiation by means of FTIR spectroscopy and SEM-EDS microanalysis. *Anal. Bioanal. Chem.* **2005**, *382*, 269–274.

26. Franquelo, M.L.; Duran, A.; Herrera, L.K.; Jimenez de Haro, M.C.; Perez-Rodriguez, J.L. Comparison between micro-Raman and micro-FTIR spectroscopy techniques for the characterization of pigments from Southern Spain Cultural Heritage. *J. Mol. Struct.* **2009**, *924–926*, 404–412.

27. Miliani, C.; Rosi, F.; Daveri, A.; Brunetti, B.G. Reflection infrared spectroscopy for the non-invasive in situ study of artists' pigments. *Appl. Phys. A Mater. Sci. Process.* **2012**, *106*, 295–307.

28. Bell, I.M.; Clark, R.J.H.; Gibbs, P.J. Raman spectroscopic library of natural and synthetic pigments (pre- ~1850 AD). *Spectrochim. Acta Part A* **1997**, *53*, 2159–2179.

29. Ambers, J. Raman analysis of pigments from the Egyptian Old Kingdom. *J. Raman Spectrosc.* **2004**, *35*, 768–773.

30. Edwards, H.G.M.; Jorge Villar, S.E.; David, A.R.; de Faria, D.L.A. Nondestructive analysis of ancient Egyptian funerary relics by Raman spectroscopic techniques. *Anal. Chim. Acta* **2004**, *503*, 223–233.

31. Lee, L.; Quirke, S. 'Painting Materials' in *Ancient Egyptian Materials and Technology*; Nicholson, P.T., Shaw, I., Eds.; Cambridge University Press: Cambridge, UK, 2000; pp. 104-120.

32. Bianchetti, P.; Talarico, F.; Vigliano, M.G.; Fuad Ali, M. Production and characterization of Egyptian blue and Egyptian green frit. *J. Cult. Herit.* **2000**, *1*, 179–188.

33. Scott, D.; Swartz Dodd, L.; Furihata, J.; Tanimoto, S.; Keeney, J.; Schilling, M.R.; Cowan, E. An ancient Egyptian cartonnage broad collar—Technical examination of pigments and binding media. *Stud. Conserv.* **2004**, *49*, 177–192.

34. Kendrick, E.; Dann, K.S.E. Structure and colour properties in the Egyptian blue family, $M_{1-x}M'_xCuSi_4O_{10}$, as a function of M, M' where M, M' = Ca, Sr and Ba. *Dye. Pigment.* **2007**, *73*, 13–18.

35. Lau, D.; Kappen, P.; Strohschnieder, M.; Brack, N.; Pigram, P.J. Characterization of green copper phase pigments in Egyptian artifacts with X-ray absorption spectroscopy and principal component analysis. *Spectrochim. Acta Part B* **2008**, *63*, 1283–1289.

36. Jaksch, H.; Seipel, W.; Weiner, K.L.; El Goresy, A. Egyptian blue—Cuprovarite a window into ancient Egyptian technology. *Die Nat.* **1983**, *70*, 525–535.

37. Mirti, P.; Appolonia, L.; Casoli, A.; Ferrari, R.P.; Laurenti, E. Spectrochemical and structural studies on a Roman sample of Egyptian blue. *Spectrochim. Acta* **1995**, *51*, 437–446.

38. Giménez, J.; Espriu-Gascon, A.; Bastos-Arrieta, J.; Joande, P. Effect of NaCl on the fabrication of the Egyptian blue pigment. *J. Archaeol. Sci. Rep.* **2017**, *14*, 174–180.

39. Schiegl, S.; Weiner, K.L.; El Goresy, A. Composition and provenance of blue and green Cu-pigments in Ancient Egyptian wall paintings: A key to the accurate chronology of bronze technology of in Ancient Egypt. *Erzmetall* **1990**, *43*, 265–272.

40. Hatton, G.D.; Shortland, A.J.; Tite, M.S. The production technology of Egyptian blue and green frits from second millennium BC Egypt and Mesopotamia. *J. Archaeol. Sci.* **2008**, *35*, 1591–1604.

41. Pagès-Camagna, S.; Colinart, S.; Coupry, S. Fabrication process of archaeological Egyptian blue and green pigments enlightened by Raman Microscopy and Scanning Electron Microscopy. *J. Raman Spectrosc.* **1999**, *30*, 313–317.

42. Colinart, S.; Pagès-Camagna, S. Egyptian Polychromy: Pigments of the pharaonic palette. In *The Polychromy of Ancient Sculptures and Terracott ARmy of the First Chinese Emperor*; Yongqi, Ed.; Arbeitshefte des Bayerischen Landesamt fur Denkmalplege: Munchen, DE, 2001; pp. 85–88.

43. Bonizzoni, L.; Bruni, S.; Guglielmi, V.; Milazzo, M.; Neri, O. Field and laboratory multi-technique analysis of pigments and organic paint media from an Egyptian coffin (26th Dynasty). *Archaeometry* **2011**, *53*, 1212–1230.

44. Chiari, G.; Scott, D. Pigments analysis: Potentialities and problems. *Int. J. Mineral. Crystallogr. Geochem. Ore Depos. Petrol. Volcanol. Appl. Top. Environ. Archaeom. Cult. Herit.* **2004**, *73*, 227–237.

45. Daniels, V.; Stacey, R.; Middleton, A. The blackening of paint containing Egyptian blue. *Stud. Conserv.* **2004**, *49*, 217–230.

46. Felder-Casagrande, S.; Wiedemann, H.G.; Reller, A. The calcination of limestone—The past, the presence and the future of a crucial industrial process. *J. Therm. Anal.* **1997**, *49*, 971–978.

47. Mazzeo, R.; Prati, R.; Quarante, M.; Joseph, E.; Kendix, E.; Galeotti, M. Attenuated reflection micro FTIR characterization of pigment-binder interaction in reconstructed paint films. *Anal. Bioanal. Chem.* **2008**, *392*, 65–76.

48. Ménager, M.; Azémard, C.; Viellescazes, C. Study of Egyptian mummification balms by FT-IR spectroscopy and GC-MS. *Microchem. J.* **2014**, *114*, 32–41.

49. Sotiropoulou, S.; Papliaka, Z.E.; Vaccari, L. Micro FTIR imaging for the investigation ofdeteriorated organic binders in wall painting stratigraphy of different techniques and periods. *Microchem. J.* **2016**, *124*, 559–567.

50. Ribechini, E.; Orsini, S.; Silvano, F.; Colombini, M.P. Py-GC/MS, GC/MS, and FTIR investigations on LATE Roman-Egyptian adhesives from opus sectile: New insights into ancient recipes and technologies. *Anal. Chim. Acta* **2009**, *638*, 79–87.

51. Pironzo, R.; Armetta, F.; Saladino, M.L.; Oliveri, F.; Tusa, S.; Caponetti. Application of Gas Chromatography coupled with Mass Spectroscopy (GC/MS) to the analysis of archeological ceramic amphorae belonging to the Carthaginian fleet that was defeated in the Egadi battle (241 B.C.). *Acta IMEKO* **2017**, *6*, 67–68.

52. Lucejko, A.J.J.; Colombini, M.P.; Ribechini, E. Chemical alteration patterns of ancient Egyptian papyri studied by Pyrolysis-GC/MS with in situ silylation. *J. Anal. Appl. Pyrolysis* **2020**, *152*, 104967, https://doi.org/10.1016/j.jaap.2020.104967.

53. van Keulen, H.; Schilling, M. AMDIS & EXCEL: A Powerful Combination for Evaluating THM-Py-GC/MS Results from European Lacquers. *Stud. Conserv.* **2019**, *64*, S74–S80.